[11]Lovell, D. A., "A Wind-Tunnel Investigation of the Effects of Flap Span and Deflection Angle, Wing Planform and a Body on the High-Lift Performance of a 28 degrees Swept Wing," Aeronautical Research Council, ARC CP-1372, London, 1977.

[12]Lovell, D. A., "A Low-Speed Wind-Tunnel Investigation of the Tailplane Effectiveness of a Model Representing the Airbus Type of Aircraft," Royal Aircraft Establishment, RAE Technical Rept. 69077, London, 1969.

[13]Kirby, D. A., and Hepworth, A. G., "Low-Speed Wind-Tunnel Tests of the Longitudinal Stability Characteristics of Some Swept-Wing Quiet Airbus Configurations," Royal Aircraft Establishment, RAE Technical Rept. 76029, London, 1976.

[14]Aiken, T. N., and Soderman, P. T., "Full-Scale Wind-Tunnel Tests of a Small Unpowered Jet Aircraft with a T-Tail," NASA-TN-D-6573, 1971.

[15]Aiken, T. N., and Page, V. R., "Stability And Control Characteristics of a Large Scale Deflected Slipstream STOL Model with a Wing of 5.7 Aspect Ratio," NASA-TN-D-6393, 1971.

[16]Page, V. R., Deckert, W. H., and Dickinson, S. O., "Large-Scale Wind-Tunnel Tests of a Deflected Slipstream STOL Model with Wings of Various Aspect Ratios," NASA-TN-D-4448, 1968.

[17]Gentry, G. L., Hammond, A. D., and Margason, R. J., "Longitudinal Stability and Control Characteristics of a Powered Model of a Twin-Propeller Deflected-Slipstream STOL Airplane Configuration," NASA-TN-D-3438, 1966.

[18]Page, V. R., and Weiberg, J. A., "Large-Scale Wind Tunnel Tests of a Airplane Model with an Unswept, Aspect-Ratio-10 Wing, Four Propellers, Blowing Flaps," NASA-TN-D-25, 1959.

[19]Chrisenberry, H. E., Doss, P. G., Kressly, A. E., Prichard, R. D., and Thorndike, C. S., "The Results of a Low Speed Wind Tunnel Test to Investigate the Effects of Installing Refan JT8D Engines on the McDonnell Douglas DC-9-30," NASA-CR-121220, 1973.

[20]Curtis, M. F., and Dent, M. M., "A Method of Estimating the Effect of Flaps on Pitching Moment and Lift on Tailless Aircraft," Royal Aircraft Establishment, RAE Rept. Aero 1861, London, 1943.

Euler Solutions for a Medium-Range Cargo Aircraft

Cengizhan Bahar,* Nafiz Alemdaroğlu,† and Yusuf Özyörük‡
Middle East Technical University, 06531 Ankara, Turkey
and
Emre Temel§
Aselsan, Inc., 06172 Ankara, Turkey

Introduction

COMPUTATIONAL fluid dynamics (CFD) has advanced rapidly as a discipline and is being increasingly used to complement the wind-tunnel measurements of complete aircraft configurations. Wind-tunnel tests are often limited by instrumentation constraints, precise model manufacturing, tunnel calibration, flow quality, wall and support interferences, and aeroelastic effects. Compared to wind-tunnel tests, CFD analyses are less expensive and require less time.

Received 6 January 2002; presented as Paper 2002-0402 at the AIAA 40th Aerospace Sciences Meeting and Exhibit, Reno, NV, 14–17 January 2002; revision received 20 October 2002; accepted for publication 2 December 2002.

*Graduate Student, Department of Aerospace Engineering; currently Engineer, Roketsan, Inc., Elmadag, 06780 Ankara, Turkey.

†Professor, Department of Aerospace Engineering. Member AIAA.

‡Associate Professor, Department of Aerospace Engineering.

§Engineer, MST Division, Systems Engineering Department, PK 101.

This Note focuses mainly on the modeling of complex, three-dimensional flowfields around a medium-range cargo aircraft, CN-235 (Ref. 1). Inviscid, subsonic flow solutions for the cargo aircraft were obtained at cruise and high-lift configurations using a commercial CFD code. The code is briefly described in the next section. The results are presented, and some conclusions are drawn from the study.

CFD Solver

Computations were done using the commercially available CFD-FASTRAN™ V2.2 code[2] employing unstructured grid methodology. The CFD-FASTRAN-V2.2 code is an implicit/explicit, upwind, cell-centered, Euler/Navier–Stokes flow solver based on finite volume method. Only the full-implicit scheme was used for all of the computations presented in this Note. The unstructured grids were generated using the commercial grid-generation code, CFD-GEOM™ V5, employing the advancing front method.[3,4] For computing flows over complex geometries, the use of unstructured grids offers considerable savings in the number of grid points and reduces the grid-generation time.[5] The geometry of the aircraft was modeled using the I-DEAS™ CAD tool.

Results and Discussion

The geometry of the conventional type, medium-range cargo aircraft, CN-235, is shown in Fig. 1. The solution model assumes no aileron, elevator, or rudder deflections. The landing gear and the propeller are also omitted, but the gondola and the engine nacelle (with blocked air intake) are retained. In the high-lift configuration study inboard and outboard wings with single-slotted flaps and flap-hinge fairings are also modeled. The overall length of the aircraft is 21.4 m, full wingspan is 25.81 m, and the root chord is 3.0 m. The aircraft has a cantilever high-wing monoplane and raked wing tips. The wing is set to a 3-deg incidence angle and has NACA65$_3$-218 wing sections.

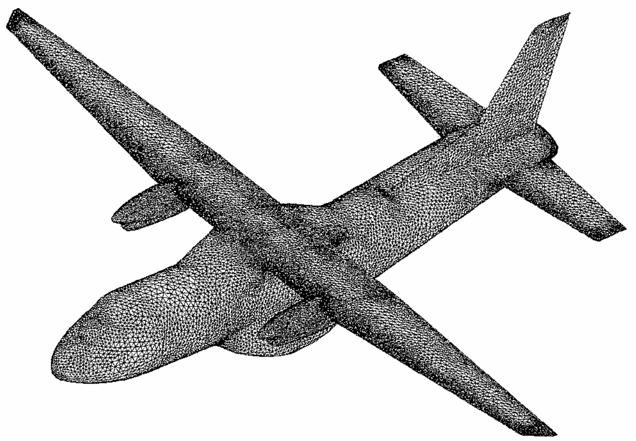

Fig. 1 Surface grid on the aircraft at cruise condition.

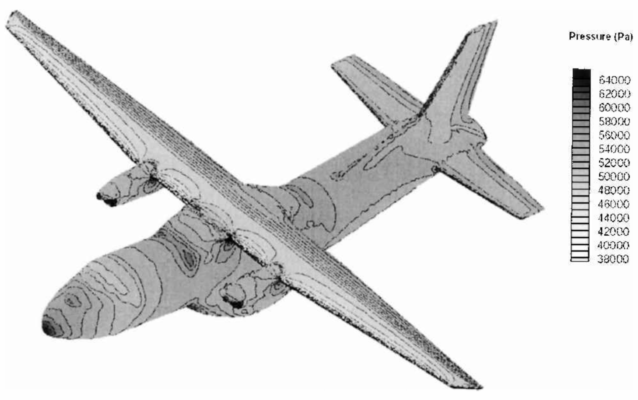

Fig. 2 Pressure contours on the aircraft at cruise condition, $\alpha = 5$ deg and $P_\infty = 57{,}207$ Pa.

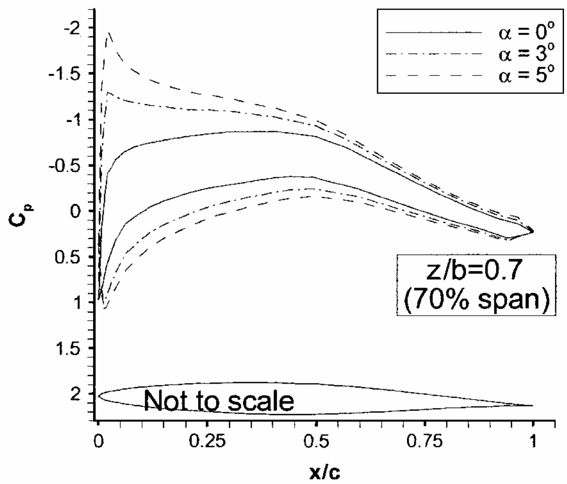

Fig. 3 Chordwise C_p distribution for cruise aircraft at various angles of attack: $P_\infty = 57{,}207$ Pa and $M_\infty = 0.39$.

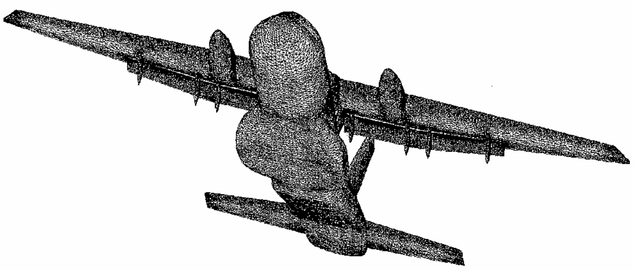

Fig. 4 Surface grid on the aircraft at landing configuration.

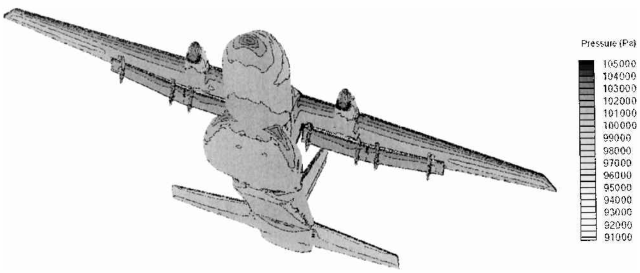

Fig. 5 Pressure contours on the aircraft at landing configuration: $\alpha = 7.5$ deg, $P_\infty = 101{,}325$ Pa, and $M_\infty = 0.163$.

After a series of grid-independence-studies, a computational domain of $7 \times 6 \times 3$ body lengths in the streamwise, vertical and spanwise directions, respectively, was found to be adequate for the computations presented in this paper. Figure 1 shows the surface grid distribution for the cruise configuration of the aircraft. The grid was generated with utmost care to avoid unnecessary grid clustering at locations far away from the aircraft while maintaining sufficient clustering near it.

Cruise Configuration

For the cruise configuration (flaps retracted) the computational grid was composed of 1,262,283 cells and 203,567 points, 46,307 of which laid on the aircraft surface. The computational results were obtained at angles of attack of 0, 3, and 5 deg and $M_\infty = 0.39$. The resultant pressure contours on the aircraft at 5-deg angle of attack are shown in Fig. 2. Stagnation points around the aircraft nose, engine inlet, and wing-aircraft intersection are evident. Figure 3 illustrates the effect of the angle of attack on the chordwise pressure coefficient C_p distribution at the 70% spanwise location. The $\alpha = 0$ deg case produced a mild expansion around the leading edge followed by a monotonic recovery to the trailing-edge pressure. As the angle of attack is increased, the pressure begins to decrease rapidly around the upper surface leading edge, and the suction peak

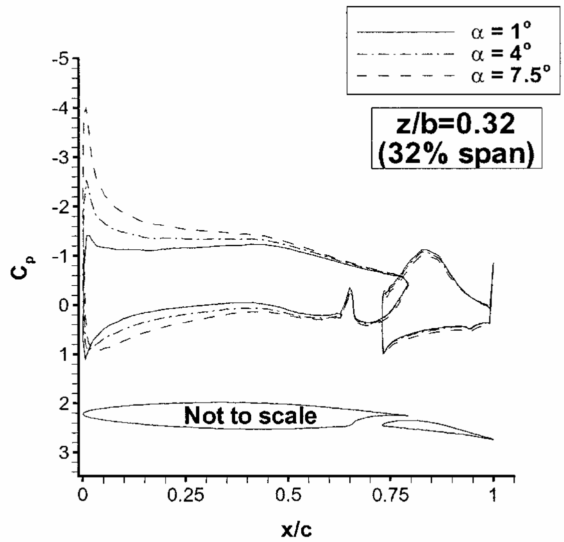

Fig. 6 Chordwise C_p distribution for landing aircraft at various angles of attack: $P_\infty = 101{,}325$ Pa and $M_\infty = 0.163$.

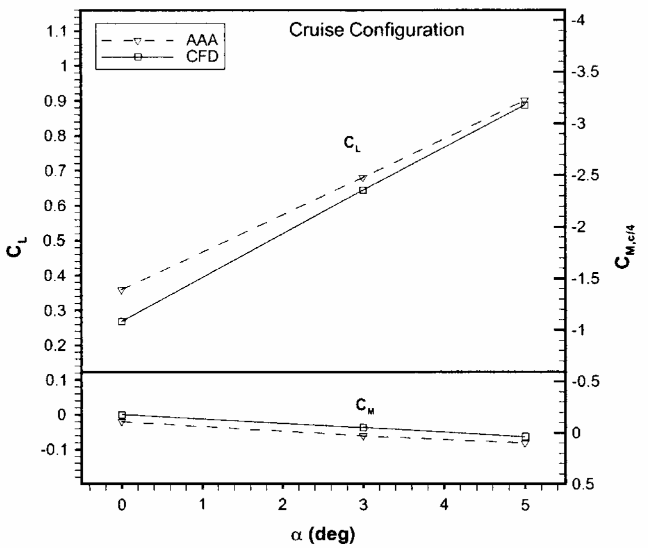

a)

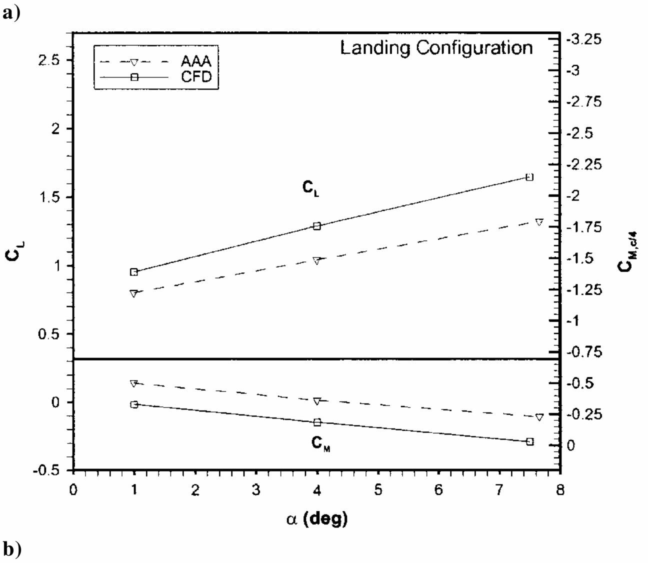

b)

Fig. 7 Comparison of aerodynamic coefficients given by the Advanced Aircraft Analysis software and CFD solutions. a) Cruise configuration: $M_\infty = 0.39$ and $\rho_\infty = 0.771$ kg/m^3 and b) Landing configuration: $M_\infty = 0.163$ and $\rho_\infty = 1.225$ kg/m^3.

values reach very low-pressure values with peak locations moving downstream.

High-Lift Configuration

For the high-lift configuration the flaps were considered to be deflected 23 deg downward (landing mode). Solutions were obtained at $\alpha = 1$, 4, and 7.5 deg on a mesh having a total of 1,467,309 cells and 242,984 points, with 72,615 points on the aircraft surface. The surface grid is shown in Fig. 4. Figure 5 shows the pressure contours on the aircraft at $\alpha = 7.5$ deg. C_p distributions at various angles of attack are given at the 32% spanwise location in Fig. 6. It is clear that the freestream angle of attack has no significant effect on the pressure distribution on the surface of the flaps. Because at this relatively high flap deflection angle, flow over the flaps is insensitive to any change in the angle of attack.

Because no experimental data on the aircraft configuration studied were available in the open literature, the CFD results were compared with the results of Ref. 6 using the Advanced Aircraft Analysis Software. This software is based on the lifting-line theory and semi-empirical formulations, which are commonly used in preliminary aircraft design.[7] As shown in Fig. 7, both of the methods show linear variations for all aerodynamic coefficients with angle of attack, having nearly the same slopes for C_M but slightly different slopes for C_L.

Computational Details

The aircraft solutions were obtained with approximately 1000 iterations for a residual reduction of about 1.5 orders of magnitude. Cruise configuration solutions of the aircraft took about one week for each angle of attack and required 1103 MB of memory on an HP-UX workstation. For the high-lift configuration solutions took about two weeks for each angle of attack and required 1275 MB of memory. It was observed that the memory requirement of the code was directly proportional to the number of cells in the computational domain.

In this work the Courant–Friedrichs–Lewy (CFL) number was varied from 1 to a final value of 100. However, when convergence problems were encountered the upper limit for the CFL number was reduced to 50 or 25. The explicit Runge–Kutta and point implicit schemes had convergence problems in all of the cases. For this reason a fully implicit scheme was used in all of the computations, although it required more computer memory.

Conclusions

Inviscid, subsonic flow solutions for a medium-range cargo aircraft were obtained on unstructured grids at cruise and high-lift configurations. From geometry modeling to the flow solution, this study was performed using the CFD-GEOM-V5 grid-generation code and the CFD-FASTRAN-V2.2 flow solver code.

The results showed that the lift coefficients varied linearly for the cruise and landing configurations. The pitching-moment coefficients showed the characteristics of a stable aircraft. Comparison of the CFD and the empirical solutions indicated a reasonable agreement for the lift and moment coefficients.

References

[1] Bahar, C., "Euler Solutions for a Medium Range Cargo Aircraft," M.S. Thesis, Dept. of Aerospace Engineering, Middle East Technical Univ., Ankara, Turkey, Jan. 2001.

[2] CFD-FASTRAN User Manual, Ver. 2.2, CFD Research Corp., Huntsville, AL, 1998.

[3] CFD-GEOM User Manual, Ver. 5, CFD Research Corp., Huntsville, AL, 1998.

[4] CFD-GEOM Tutorials, Ver. 5, CFD Research Corp., Huntsville, AL, 1998.

[5] Dodbcle, S. S., "Three Dimensional Aerodynamic Analysis of a High-Lift Transport Configuration," AIAA Applied Aerodynamic Conference, AIAA Paper 93-3536, Monterey, CA, Aug. 1993.

[6] Karaağaç, C., "The Aerodynamics, Flight Mechanics and Performance Predictions for a Medium Range Cargo Aircraft," M.S. Thesis, Dept. of Aerospace Engineering, Middle East Technical Univ., Ankara, Turkey, Nov. 1998.

[7] Roskam, J., *Airplane Design*, Roskam Aviation and Engineering Corp., Ottowa, KS, 1985.

Analytical Representation of Aerodynamic Forces in Laplace Domain

Bertil A. Winther*
The Boeing Company,
Huntington Beach, California 92647-2048

Nomenclature

$\boldsymbol{A}_k$	=	system matrix for model k
$\boldsymbol{C}$	=	general matrix $\boldsymbol{M}$ or $\boldsymbol{P}$
D	=	determinant of dynamic system
E_i	=	aerodynamic coefficients due to pitch
h	=	vertical position coordinate
$\boldsymbol{I}$	=	identity matrix
ℓ	=	reference length
$\boldsymbol{M}$	=	mass matrix
N_n	=	numerator terms in response equation
$\boldsymbol{P}$	=	complex aerodynamic force matrix
p_j	=	aerodynamic pressure on surface
$\boldsymbol{Q}$	=	aerodynamic force matrix in Laplace domain
q	=	pitch rate at c.g.
S	=	area of surface exposed to airflow
s	=	Laplace variable
t	=	time
U	=	mean velocity of airflow
w	=	downwash on aircraft surface
$\boldsymbol{X}_k$	=	state-variable vector for model k
x, y, z	=	aircraft mean-flight-path axes
α	=	angle of attack at c.g.
Δn_z	=	incremental load factor at c.g.
δ	=	control surface deflection
ζ	=	displacement in z direction
θ	=	pitch angle
λ	=	complex eigenvalue
μ	=	structural mass density
τ	=	reference time
Φ_j	=	shape of mode j
ω	=	circular frequency

Subscripts

h	=	control surface hinge value
i, j	=	modal indices
s	=	steady-state value
0	=	value at aircraft c.g.

Superscript

T	=	transposed matrix

Introduction

TO predict aeroelastic stability and response, the equations of motion (EOM) normally are formulated in the frequency domain. In accordance with the small-displacement theory, a linear

Received 20 December 2001; revision received 6 October 2002; accepted for publication 18 November 2002.

*Senior Principal Engineer, Phantom Works, Loads, and Dynamics.